Peeling of polydimethylsiloxane adhesives at low velocities: cohesive failure

Jean-Michel Piau, Guillaume Ravilly, Claude Verdier

PEELING OF POLYDIMETHYLSILOXANE ADHESIVES AT LOW VELOCITIES: COHESIVE FAILURE

J.-M. Piau, G. Ravilly

Laboratoire de Rhéologie
(Universités de Grenoble UJF-INPG and CNRS, UMR5520)
BP 53 – Domaine Universitaire
38041 Grenoble cedex 9
France

C. Verdier*

Laboratoire de Spectrométrie Physique
(Université de Grenoble UJF and CNRS, UMR5588)
BP 87 – 140 avenue de la Physique
38402 Saint-Martin d'Hères
France

ABSTRACT:

This work presents results obtained in 90-degree peeling tests at low velocities in the case of Newtonian adhesives, when failure is cohesive. Peeling experiments are described and consider the influence of the thickness, viscosity and surface tension of the adhesive, as well as the backing rigidity.

A simple model, based on lubrication effects in thin films, is considered and compared with the measurements, when peeling is a two-dimensional phenomenon. Furthermore, a criterion for predicting the transition between the two dimensional regime and the three dimensional one at higher velocities is proposed.

* Corresponding author. verdier@ujf-grenoble.fr

1. INTRODUCTION

The knowledge of the adhesive properties requires the determination of its stickiness using standard tests. This can be done using a double cantilever beam test [1], a modified JKR test [2] and other kinds of experiments like tack and peel. The tack test consists in bringing a solid probe into contact with a pressure sensitive adhesive (P.S.A.) for a short time and then withdrawing it [3]. By varying the pulling velocity, the pressure and the contact time, this test allows to measure the maximum force or energy to break the bond. Peel tests, on the other hand, are carried out after forming a bond by setting an adhesive (with backing) onto a pre-treated surface. Then the adhesive/backing compound is pulled away at constant angle (usually 90°) and the energy restitution rate (force per unit width) is obtained. Special peel tests can provide data over a large range of velocities or reduced velocities [4], as long as the time temperature superposition principle holds for the adhesive considered

Surface treatments are also necessary before carrying out tests, to avoid pollution and to provide reproducible surfaces. Different types of treatments are available such as mechanical, chemical, flame, plasma or UV treatments, all depending on the nature of the surfaces. Indeed, chemical treatments will be more adequate for metallic surfaces while Corona discharge or flame treatments are preferred for solid polymer surfaces [5]. As a result, various techniques are used to evaluate the effect of surface changes after treatment: X-Ray Photoelectron Spectroscopy (XPS) is a method for investigating the different components or elements present at the surface, as well as Auger electron spectroscopy, ion scattering spectroscopy or even acoustic scanning microscopy [6]. Free surface energies are also very important and can be determined by conventional wetting measurements with different liquids, using dispersive and polar decomposition [7-8]) or acid-base decomposition [9].

Many works, theoretical as well as experimental, have focused on peel adhesion. In particular, the general shape of the curve showing the energy release rate G as a function of velocity V depends on the type of adhesive and upon the polymer degree of cross-linking. Generally, one finds one branch for cross-linked adhesives, corresponding to interfacial peeling (low surface energy) or cohesive peeling (high surface energy) [10]. In the case of uncrossed-linked adhesives, which is more common, there are two branches, a cohesive and an interfacial one.

At low velocities or high temperatures, i.e. the cohesive regime, Benyahia et al. [11] observed the mechanisms of peeling, and obtained the general shape of peeling master curves in a log-log plot (Fig. 1). One can recognize three regimes: at very low velocities (regime

C0), G is a roughly a constant. After a typical velocity V1, a second regime (C1) shows increasing G with a slope of 0.6, corresponding to a two-dimensional flow of the adhesive. Finally, regime C2 starts at velocity V2, with G increasing with a slope 0.8, and this three-dimensional flow is characterized by the formation of regularly spaced filaments.

At very low speeds (regime C0), several authors tried to relate the plateau for G with the physico-chemical aspects. Gent and Schultz [12] showed that the peel strength G is a product of two terms, one depending on surface energies, the other one being a rheological function $\phi(a_T V)$ of the adhesive due to the energy dissipated irreversibly in the bulk. This function should go to 1 when $a_T V$ goes to 0 :

$$G = G_0\left(\phi(a_T V)\right) \tag{1}$$

where a_T is a function of temperature and $a_T V$ is the reduced peeling velocity. When failure is at the interface, G_0 is close to the Dupré work of adhesion $\omega_a = \gamma_a + \gamma_s - \gamma_{as}$ where γ_a and γ_s are respectively the free energies of the adhesive and substrate, and γ_{as} the interaction energy. In cohesive failure, ω_a is replaced by the cohesive energy $\omega_c = 2\gamma_a$. Carré and Schultz [13], after studying the separation of aluminium/elastomer model assemblies in air and liquid media, proposed to replace G_0 by $W_0^c\, g(M_c)$ where W_0^c is the reversible energy of cohesion measuring the energy required to break all physical and chemical bonds per unit area ($W_0^c = \omega_c + W_{0chem}^c$, where W_{0chem}^c are chemical interactions or entanglements). $g(M_c)$ is a molecular dissipation factor related to the irreversible deformation of bonds in the chains between two cross-links and M_c is a homogeneous distribution of cross-links. One of the questions which remains is the generality of this formula, as well as the zero velocity limit, if measurable. Finally, the determination of $\phi(a_T V)$ is still under way but remains a major difficulty.

In regime C1, there are not many studies dealing with the prediction of cohesive flow. The major work is by Kaelble [4], using Bikerman's works [14-15], who proposed a theoretical model when the adhesive is Newtonian.

When two-dimensional peeling becomes unstable (regime C2) at velocity V2, the instability gives rise to regularly spaced ribs. This regime is comparable to hydrodynamic instabilities previously described [16-17], when investigating the flow of Newtonian fluids between counter rotating rollers. Empirical formulae predict the velocity of appearance of the ribs as well as their periodicity. Such formulae may be applied to the adhesive peeling case. Regime C2 has been the subject of numerous works. Kaelble predicted experimentally the distribution of cleavage stresses [18] at the adhesive-substrate interface and showed that the

contribution to peel force by filamentation is significant. Niesiolowski and Aubrey [19] introduced the filamentation effect at the peeling front and measured the backing curvature to determine peel force. Zosel observed the filamentation mechanisms in a tack experiment [20] and pointed out the importance of the elongational properties of adhesives. Gent and Petrich [21] approximated the deformation of an adhesive (during peel) to a uniaxial elongation, and predicted peel force from extensional rheometry data. Verdier et al. [22] finally proposed a model to determine the peeling energy using both shear and elongational rheometrical data as well as physical observations.

In this paper, we compare experimental peeling data with an analytical model based on lubrication assumptions, allowing the different parameters to vary (adhesive thickness, viscosity, surface tension, and backing elasticity). Then we investigate the transition between C1 and C2. In the first part, we derive a theoretical relationship between the energy restitution rate G and the peeling velocity V as well as the other parameters (regime C1). In the next part, we give details of the experimental setup and results, in particular peeling curves. Finally, we use our results and previous data to obtain a reduced peeling master curve based on our theoretical analysis. The criterion for predicting the transition from C0 to C1 is also presented.

2. THEORETICAL PEELING MODEL

A schematic view of the adhesive joint in the peeling zone is represented in Fig. 2. Then we will make the following hypotheses:

a) The backing is a flexible elastic strip (much longer and wide than thick) whose deformation is assumed to be one-dimensional and governed by standard beam theory.

b) The adhesive is Newtonian and undergoes two-dimensional cohesive failure at constant temperature.

c) Lubrication theory for the flow of the adhesive is assumed, i.e. the velocity distribution u(y) is one-dimensional and depends on the y-coordinate only.

Under these assumptions, a rather lengthly calculation can be carried out, whichis presented in the appendix 1, and one recovers the force F, or the energy restitution rate G, as a function of the relevant parameters

$$G = \frac{F}{b} = K\left(E^{\frac{3}{7}} h^{\frac{9}{7}} e^{-\frac{6}{7}} \eta^{\frac{4}{7}} V^{\frac{4}{7}} \right) \qquad (2)$$

where b is the adhesive strip width, E the elastic modulus of the backing, h the half-thickness of the backing, η the adhesive viscosity, V is the peeling velocity and K is a constant.

Further comparisons with other previous works can now be made. The first attempt to predict peeling force was made by Bikerman [14], who proposed a relationship linking the force required to peel a Hookean adhesive between a rigid plate and a flexible ribbon. He found:

$$\frac{F}{b} = 0.3799\, \sigma\, e^{\frac{1}{4}} h^{\frac{3}{4}} \left(\frac{E}{Y}\right)^{\frac{1}{4}} \tag{3}$$

where Y is the Young modulus of the ribbon and σ the tensile strength of the adhesive layer. This is of course rather out of the scope of our analysis, but still an interesting result. Kaelble indeed used Bikerman's equation and wrote a general relation for the peel force when the adhesive is Newtonian [4]:

$$F = \left(12 \frac{K}{t_m} \frac{\eta b}{e} EI\right)^{\frac{1}{2}} \tag{4}$$

where $\frac{K}{t_m}$ is a peel rate factor and t_m, a typical time, is determined by the rate at which the viscous fluid can follow the movement of ribbon. This equation may also be rewritten (using the formula for I) :

$$\frac{F}{b} = 2\sqrt{2} \left(\frac{E\, h^3}{e}\right)^{\frac{1}{2}} \eta^{\frac{1}{2}} \left(\frac{K}{t_m}\right)^{\frac{1}{2}} \tag{5}$$

It is now in a convenient form to be compared with (2), after we make an assumption for $\frac{K}{t_m}$.

From [4], it seems reasonable to assume that t_m varies like $\frac{e}{V}$, the typical experimental time scale. This would lead to a power law dependence of (ηV) with exponent ½ (compared to 4/7 in Eq. (2)) and for the thickness e, the exponent would be –1 (to be compared with –6/7 in Eq. (2)). Other parameters also give reasonable comparisons. To validate our model, we will now compare our scaling law with the experimental results.

3. EXPERIMENTAL MEASUREMENTS

3.1. Experimental setup

We start here with a brief description of the materials which are used throughout this study. We used two PDMS (polydimethylsiloxane), A and B, as adhesives. Measurements using another adhesive (C) will also be reported and are taken from a previous study [11].

Regarding backings, three different ones are used, one made of Polyester, and two out of steel with different thicknesses. The characteristics of the adhesives and backings are reported respectively in Tables 1 and 2. The main advantage of using PDMS is that it behaves as a Newtonian fluid in the range of velocities considered here. Moreover, precise rheometrical data has been obtained previously, as given by dynamic shear master curves covering ten decades in frequency [23].

Adhesives are coated using a blade device. This apparatus allows us to control thickness. PDMS is applied first on the backing, placed horizontally. Then the backing is pulled slowly under a blade. This blade is held fixed on calibrated magnets, which allow maintaining a well-determined gap. After coating is achieved, we measure the weight of the assembly to check the adhesive thickness. Adhesive strips, obtained using this process, are then smoothly applied onto a Pyrex™ surface. The latter one has been treated carefully by successive degreasing, sulfochromic etching, rinsing and vacuum drying. Note that this procedure is standard in our tests but is not fundamental here since failure is cohesive, i.e. not located at the interface.

The 90° peeling experiments have been described precisely by Benyahia et al. [11]. The system is made of two micrometric tables moving at the same controlled velocity V in the horizontal and vertical directions. The substrate is fixed on the horizontal table and the force transducer (measuring the force F) is fixed on the vertical one. The adhesive strip is set on the substrate under controlled pressure and attached to the transducer so that the peeling front is always fixed in the laboratory reference frame. The whole system is put into a chamber where temperature (T) is controlled as well as the relative humidity (RH).

For the very low speeds, we had to modify our instrumentation because of the low values of the force. We replaced the force transducer (sensitivity 0.1g) by an electronic weighting unit (sensitivity 0.001g) for increased accuracy.

3.2. Peeling curves

All experiments are carried out at a temperature of 20°C and a relative humidity around 10 %. After setting up the adhesive strip, we wait for two hours until equilibrium is reached. Peeling starts by moving the two tables at the same moderate velocities, in order to create the adhesive free surface at the peeling front. The system is then stopped. After a short time, we start a new peeling at the required velocity V and follow the force signal. The latter one shows a transient regime first, which corresponds to deformation of the free surface, and then it reaches a constant value representing the peel force F(V). The time required to reach this steady state regime is inversely proportional to the peeling velocity and depends on the initial

conditions i.e. the shapes of the peeling front and backing. At very low speeds, when long times are required, the force signals are not constant but increase slightly linearly due to the increase of adhesive/backing weight, so we need to apply a weight correction to the measured force. The energy release rate G is plotted as a function of velocity V :

$$G = \frac{F}{b} = G(V) \tag{6}$$

where b is the width of the adhesive strip.

As discussed above, the conditions at the beginning of a peeling experiment are very important especially at very low speeds when the energy restitution rate is of the same order as the free surface energy of the adhesive. In order to validate this principle, two types of experiments with different initial conditions were conducted (Figs 3a-b). In case (a), we take into account the creation and deformation of the free surface at the peeling front whereas in case (b), we only have a deformation of this free surface. The same behaviors for cases (a) and (b) (Fig. 4) are observed for the high velocities, as expected. At low velocities, on the other hand, there are differences, due to the fact that the creation of the free surface (a) is energy consuming. In the experiments that will follow, we will retain case (b) which corresponds to reproducible free surfaces obtained by peeling at the same moderate speed for each series of tests, before measuring the peel force at the desired velocity. Let us note that the value of the magnitude of the so-called "plateau" in the low velocity regime (Fig. 1) is hard to obtain precisely [11] but is roughly in the range of the adhesive cohesive energy, i.e. 42 mN/m in this case. A different method is still required to be able to reach the plateau limit.

3.2.1. Influence of adhesive viscosity (η)

We first achieve two series of measurements using a polyester backing (P23 in Table 2) and adhesives A and B (thickness obtained from coating e = 80 ± 7 μm). Figure 5 shows the peeling curves of PDMS on a Pyrex™ substrate. Measurements have been carried out at T = 20 ± 0.1 °C with a relative humidity RH = 10 ± 5 %. For all these experiments, failure takes place in a cohesive manner.

Let us look at the behavior of adhesive A. First of all, at very slow peeling velocities (1.10^{-6} m.s^{-1} ≤ V ≤ 5.10^{-5} m.s^{-1}), we observe two-dimensional flow at the peeling front (C1) as described previously [11], this regime is associated with a slope of 0.6 in a logarithmic scale. As we move along the peeling curve, increasing peel rate, we notice a transition region, i.e. an unstable zone where the two-dimensional flow tries to become a three-dimensional one without reaching steady state. Moreover, the measured force is not constant but decreases

with the appearance of ribs and increases when ribs disappear, thus leading to an oscillatory regime of force. As we increase the speed rate (1.10^{-4} m.s^{-1} ≤ V ≤ 8.10^{-3} m.s^{-1}), beyond the transition area, we clearly observe three-dimensional flow (C2). This flow is associated to a slope of 0.8 in a logarithmic scale.

Let us now observe the results for adhesive B. Regime C1 takes place at peeling velocities between 5.10^{-7} m.s^{-1} and 8.10^{-6} m.s^{-1} (slope of 0.6) and the three-dimensional regime (C2) at peel rates between 2.10^{-5} m.s^{-1} and 2.10^{-3} m.s^{-1} (slope 0.8). Between these two regimes we find a similar transition region. The differences between these two adhesives obviously come from their different viscosities.

3.2.2. Influence of the backing rigidity (EI)

In this part, we study the influence of the backing rigidity and deal with experiments involving adhesive B and different types of backings (see Table 2). Figure 6 shows the peeling curves on a Pyrex™ substrate. Measurements have been carried out at T = 20 ± 0.1 °C and RH =10 ± 5 %. In these peeling tests, the failure mode is still cohesive.

The behavior obtained with the S20 backing is somewhat different from the other one (P23). At low velocities, we observe the typical C1 regime, but the transition has moved. After a short unstable regime, the adhesive does not obey a linear slope in the G(V) diagram. The linear regime with slope 0.8 is only obtained at higher velocities. This behavior will be discussed later in §4.

3.2.3. Influence of adhesive thickness (e)

The influence of the adhesive thickness (e) is studied by carrying out experiments using adhesive A coated on the polyester backing P23 using different thicknesses. In addition to our previous peel tests with thickness e=80µm, we used another thickness (e=160µm). These two curves (with a Pyrex™ substrate) are shown in Figure 7. Measurements have been carried out at T = 20 ± 0.1 °C and RH = 10 ± 5 %. The behavior of the adhesive strip with thickness e=160µm is the same as the adhesive strip e=80µm but corresponds to lower levels of forces. Usually, it is found that the peeling energy increases when decreasing thickness (see Eq. (5)), in the case of Newtonian adhesives. This is precisely why small thicknesses are used with common glues in order to increase adhesion.

In the next section, we will now compare theory with experiments, in order to come up with a master curve involving the different parameters above.

4. Analysis and discussion

4.1. Peeling master curve

Figure 8 shows the peeling master curve which is constructed by superposition of peeling curves obtained with adhesives A, B with different backings and different thicknesses. We have also included previous data, obtained by Benyahia et al. [11]. These measurements were carried out with adhesive C (see Table 1) using the same polyester backing but with a different thickness (e=100μm) at a temperature of 50°C. We know that adhesive C has a Newtonian behavior in the low velocity range at 50°C. This is not a problem to superpose different results at different temperatures, because in this case, the only important parameters which depend on temperature are the viscosity (η) and the surface tension (γ) of the adhesive. Therefore all we need to do is to use the relevant parameters (η,γ) at the required temperatures.

In this peeling master curve, we plotted $\xi^{3/7}$ G as a function of ηV, after using a new variable $\xi = \frac{\eta V e^2}{E h^3}$. ξ represents the viscous effects of adhesives versus the backing rigidity effects. This parameter can be introduced naturally when writing the equilibrium equation for the backing, considered as a beam, submitted to a vertical force, and in contact with the adhesive. The curves obtained superpose quite well in the C1 regime ($\eta V<10^{-2}$ N/m), but in the second regime C2 ($\eta V>10^{-2}$ N/m) they exhibit differences. Regime C1 differs from regime C2 by a different slope. Regime C1 is characterized by a slope of 1 in a logarithmic scale, according to our model. Indeed, Eq. (2) may be rewritten:

$$\xi^{3/7} G = K \eta V \tag{7}$$

Concerning regime C2, superposition of the three adhesive experiments is still good but our scaling law is no longer useful because of the three-dimensional flow and the model hypotheses. In this case, we should take into account the rib formation, where the elongation effects become dominant [22]. The constant K may actually be a function of the adhesive surface tension γ in this case. This is the only parameter which does not show in the model, and it will be introduced now. Moreover, to obtain a dimensionless representation, we have introduced the surface energy through the capillary number (Ca). For a careful analysis of the relevant dimensionless parameters, one can refer to Piau et al. [24]. We can then propose:

$$\xi^{\frac{3}{7}} \frac{G}{\eta V} = K(Ca) \tag{8}$$

where K is now a function of $Ca = \frac{\eta V}{\gamma}$, the capillary number. This representation is shown

in Figure 9. In the high velocity regime, the dependence on Ca is complex, involving minima, so we will limit ourselves to determine the average constant K in the low velocity regime (regime C1): K= 0.2 is the appropriate number. Finally, for the small velocities corresponding to our low-velocity model, we find:

$$G = 0.2\left(\frac{Eh^3}{e^2}\right)^{\frac{3}{7}}(\eta V)^{\frac{4}{7}} \tag{9}$$

It is now needed to write this relationship in terms of the dimensionless numbers ξ and Ca. Taking into account the previous observations showing the importance of the creation of a free surface (Fig. 3), we may assume that this creation (two surfaces in fact) requires an energy per unit surface equal to $w_c=2\gamma$, so that the total energy G_t becomes

$$G_t = w_c\left(1+0.1\left(\frac{Eh^3}{\eta V e^2}\right)^{\frac{3}{7}}\left(\frac{\eta V}{\gamma}\right)\right) \tag{10}$$

In this final expression, we are showing the two relevant dimensionless numbers of our problem, ξ and Ca. This formula is valid in the C1 regime and holds as long as there are no cross-linking effects or physico-chemical interactions, which might create changes in the value of w_c, as was suggested previously [13]. We believe that this relation is universal.

4.2. Critical conditions between C1 and C2

Let us now pay attention to the transition velocity from C1 to C2. Pitts and Greiller [16] measured conditions under which the ribs start to appear, in the case of a Newtonian fluid moved by counter-rotating rollers (radius R). They changed speeds (V), viscosities (η), gap width (2e) and used different liquids to investigate the effect of surface tension (γ). They obtained the following empirical formula at criticality, relating the two relevant dimensionless numbers, i.e. the capillary number Ca and a geometrical parameter e/R:

$$\frac{\eta V}{\gamma} = 62\,\frac{e}{R} \tag{11}$$

Mills and South [17] studied theoretically this problem, and found that the onset of ribbing was governed by the relation:

$$\frac{\eta V}{\gamma} = 10.3\left(\frac{e}{R}\right)^{0.75} \tag{12}$$

Both (11) and (12) were obtained using constant radius R. In our case, we may consider that the problem is similar, because it would correspond to the flow created by two rollers with different radii, one equal to R, and the other one being infinite. R is then the proper length. Furthermore, R is not a constant value here and depends on the different parameters, in

particuler the velocity V. R can be obtained experimentally by measuring the radius of curvature for $\omega=0$ in Fig.2. A circle, parabola (Eq. (A5) in appendix 1) can be used to fit the backing as well as the analytical value (Eq. (A2) in appendix 1). These methods all give similar numbers for R close to $\omega=0$ [25]. From theses values, at each different velocity, one can compute e/R and plot $Ca=\eta V/\gamma$ as a function of e/R, as shown in Fig. 10. This is done using a log-log scale and a resulting slope of about 0.5 is obtained :

$$\frac{\eta V}{\gamma} = 1.8\left(\frac{e}{R}\right)^{0.5} \tag{13}$$

This relation differs slightly from (11) and (12) but the exponent is similar and one has to realize that, in the experiments performed earlier, it has been rather difficult to have an accurate observation of the appearance of these ribs [26]. Therefore this may induce small changes in the critical velocity. Finally we conclude that our criterion (13) seems rather well adapted to the appearance of ribs in cohesive peeling of Newtonian adhesives.

5. Conclusion

In this paper, we have focused on the effects of adhesive viscosity, thickness and surface tension, as well as backing rigidity, on the peeling energy required to carry out a 90°-peel test of a Newtonian adhesive. In the low velocity regime, we found a master curve, which contains two dimensionless parameters relevant to the problem. The higher velocity case is not so simple due to the appearance of regularly spaced ribs and depends on the capillary number in a more complex manner.

The transition from the two-dimensional regime to the three-dimensional one, associated with the formation of ribs, is governed by a simple criterion relating the capillary number to a geometrical parameter, and compares well with experiments carried out with counter-rotating rollers.

These relationships may be useful to predict peel adhesion between Newtonian adhesives and may be considered as a starting point in the adhesion of more complex polymeric adhesives.

Appendix 1 : Peeling model for a Newtonian adhesive

We consider a strip of adhesive (b is the width and L the length of the front), constituted by the backing (thickness 2h) and the adhesive layer (thickness e). At one end we apply a traction force F under a constant angle of $\frac{\pi}{2}$ (Fig. 2). It follows from beam theory that in this case:

$$EI\left(\frac{d\omega}{ds}\right) = -mF \tag{A1}$$

$\omega(s)$ is defined in Figure 2. E and $I = \frac{2b\,h^3}{3}$ are respectively the modulus of elasticity and the moment of inertia of the backing, m is the moment arm of the peel force, $\frac{d\omega}{ds}$ is the curvature at curvilinear abscissa s. Following [4], we obtain the radius of curvature R, at $\omega = 0°$:

$$R = \sqrt{\frac{E\,I}{2\,F}} \tag{A2}$$

We consider a piece of flexible backing and equilibrate pressures on each side with the traction force F, thus we find :

$$F = b\,R\,\Delta p \tag{A3}$$

Δp (the variation of pressure in the adhesive layer) can be computed, using lubrication theory (e.g. L>>e and $\frac{\partial^2 u}{\partial x^2} << \frac{\partial^2 u}{\partial y^2}$, u(y) is the flow velocity), we write :

$$\frac{dp}{dx} = \eta \frac{d^2 u}{dy^2} \tag{A4}$$

where η is the viscosity of the Newtonian adhesive. In this equation, the pressure gradient $\frac{dp}{dx}$ only depends on x. To solve this equation, we use the following boundary conditions u(0)=V and u(H(x))=V. H(x) is assumed to have a parabolic shape, representing the backing, with an initial radius of curvature R, therefore :

$$H(x) = \frac{x^2}{2R} + e \tag{A5}$$

Integration of (A4) leads to:

$$u = \frac{1}{2\eta}\left(\frac{dp}{dx}\right)\left(y^2 - y\,H(x)\right) + V \tag{A6}$$

The surface flow rate of the adhesive layer is:

$$Q = V e = \int_0^{H(x)} u(y)dy = \frac{1}{2\eta}\left(\frac{dp}{dx}\right)\left(\frac{-H^3(x)}{6}\right) + V H(x) \qquad (A7)$$

This requires the pressure gradient to vary with H(x) according to the relation:

$$\frac{dp}{dx} = 12\,\eta V\left(\frac{H(x) - e}{H^3(x)}\right) \qquad (A8)$$

Integrating (A8) from 0 to L, after using (A5), we obtain:

$$\Delta p = \frac{3\eta V}{\sqrt{2}}\left(\frac{RL\left(L^2 - 2eR\right)}{e\left(2eR + L^2\right)^2} + \frac{\sqrt{R}}{e\sqrt{e}}\,\mathrm{Arc\,tan}\left(\frac{L}{\sqrt{2eR}}\right)\right) \qquad (A9)$$

Assuming that $L >> \sqrt{2eR}$ (usually true in the experiments), (A9) simply reads:

$$\Delta p = k\,\eta\,V\frac{\sqrt{R\,e}}{e^2} \qquad (A10)$$

where k is a constant, and V is the peeling velocity. Combining the equations (A2)-(A3)-(A10), we obtain a scaling law, linking force and peeling rate:

$$G = \frac{F}{b} = K\left(E^{\frac{3}{7}} h^{\frac{9}{7}} e^{-\frac{6}{7}} \eta^{\frac{4}{7}} V^{\frac{4}{7}}\right) \qquad (A11)$$

with K a constant. This equation, which links the energy release rate (G) with the peeling rate (V), takes into account the geometrical parameters, including the thickness of the adhesive layer (e) and the half thickness of the backing (h), the Young modulus of the backing (E) and the viscosity of the adhesive (η).

References

[1] Boucher E., Folkers J.P., Creton C., Hervet H., Léger L., Enhanced adhesion between polypropylene and polyamide-6 : role of interfacial nucleation of the β-crystalline form of polypropylene. Macromolecules, 30, 2102-2109, 1997.

[2] Deruelle M., Léger L., Tirell M., Adhesion at the solid-elastomer interface : influence of the interfacial chains. Macromolécules, 28(22), 7419-7428, 1995.

[3] Zosel A, Adhesion and tack of Polymers: Influence of Mechanical Properties and Surface Tensions, Coll. and Polym. Sci., 263, 541-553, 1985.

[4] Kaelble D. H., Theory and analysis of peel adhesion : mechanisms and mechanics. Trans. of the Soc. of Rheol., 3, 161-180, 1959.

[5] Brewis D.M., Briggs D., In Industrial adhesion problems, edited by Brewis D., Briggs D., Orbital Press, Oxford, 1985.

[6] Wu S., In Polymer interface and adhesion, edited by Marcel Dekker Inc, New York, 1982.

[7] Fowkes F.M, Additivity of intermolecular forces at interfaces. I. : Determination of the contribution to surface and interfacial tensions of dispersion forces in various liquid. J. Phys. Chem., 67, 2538-2541, 1962.

[8] Owens D.K., Wendt R.C., Estimation of the surface free energy of polymers. J. Appl. Polym. Sci., 13, 1741-1747, 1969.

[9] Van Oss C.J., Giese R.F., Wu W., On the predominant electron-donicity of polar solid surfaces. J. Adhesion, 63, 71-88, 1997.

[10] Verdier C., Piau J.M., Benyahia L., Peeling of acrylic pressure sensitive adhesives : cross-linked versus uncross-linked adhesives. J. Adhesion, 68, 93-116,1998.

[11] Benyahia L., Verdier C., Piau J.M., The mechanisms of peeling of uncross-linked pressure sensitive adhesive. J. Adhesion, 62, 45-73, 1997.

[12] Gent A.N., Schultz J., Effect of wetting liquids on the strength of adhesion of viscoelastic materials. J. Adhesion, 3, 281-294, 1972.

[13] Carré A., Schultz J., Polymer-aluminium adhesion II Role of adhesive and cohesive properties of the polymer. J. Adhesion, 17, 135-156, 1984.

[14] Bikerman J.J., Theory of peeling through a Hookean solid. J. Appl. Phys, 28, 1484-1485, 1957.

[15] Bikerman J.J., Yap W., Rheology of peeling in a Newtonian liquid., Trans. of the Soc. of Rheol., 2, 9-21, 1958.

[16] Pitts E., Greiller J., The flow of thin liquid films between rollers. J. Fluid Mech., 11, 33-50, 1961.

[17] Mill C.C., South G.R., Formation of the ribs on rotating rollers. J. Fluid Mech., 28, 523-529, 1967.

[18] Kaelble D.H., Reylek R.S., Peel adhesion : rate dependence of micro fracture processes. J. Adhesion, 1, 124-135, 1969.

[19] Niesiolowski F., Aubrey D.W., Stress distribution during peeling of adhesive tapes. J. Adhesion, 13, 87-98, 1981.

[20] Zosel A., Adhésion et tack des polymères. Influence des propriétés mécaniques et de la structure moléculaire. Double liaison, 431-432, 275-284, 1991.

[21] Gent. A.N., Petrich R.P., Adhesion of viscoelastic materials to rigid substrates. Proc. Roy. Soc., A 310, 433-448, 1969.

[22] Verdier C., Piau J.M., Benyahia L., Influence des propriétés élongationnelles dans le pelage des polymères. C. R. Acad. Sc. Paris, t 323, Série II b, 739-746, 1996.

[23] Longin P.Y., Verdier C., Piau M., Dynamic shear rheology of high molecualr weight polydimethylsiloxanes :comparison of rheometry and ultrasound. J. Non-Newtonian Fluid Mech., 76, 213-232, 1998.

[24] Piau J.M., Verdier C., Benyahia L., Influence of rheology and surface properties in the adhesion of uncross-linked pressure sensitive adhesives. Rheol Acta, 36, 449-461, 1997.

[25] Ravilly G., Adhésion et pelage bidimensionnel des polymères, PhD Thesis, Université de Grenoble I, 2001.

[26] Coyle DJ, Macosko CW, Scriven LE, Stability of symmetric film-splitting between counter-rotating cylinders, J. Fluid Mech., 216, 437-458 (1990)

Figure captions

Figure 1: General shape of the energy release rate G vs. peeling speed V in the cohesive failure mode.

Figure 2: Schematic cross-section of an adhesive joint in the peeling zone.

Figure 3: Schematic situations of the peeling front at the beginning of a peel test: (a) Creation and deformation of free surface. (b) Deformation of free surface only.

Figure 4: Peeling curves of adhesive A (e = 80 μm) with different initial conditions (a) and (b) on Pyrex™ substrate using polyester backing P23 (T=20°C, RH=10%).

Figure 5: Comparison of peeling curves of adhesives A and B (e = 80 μm) on Pyrex™ substrate using polyester backing P23 (T=20°C, RH=10%).

Figure 6: Peeling curves of adhesive B on Pyrex™ substrate with different backings (T=20°C, RH=10%).

Figure 7: Peeling curves of adhesive A with different thicknesses on Pyrex™ substrate using polyester backing P23 (T=20°C, %RH=10%).

Figure 8: Peeling master curve (T=20°C, RH=10%) $\xi^{3/7}G$ vs. ηV

Figure 9: Other form of peeling master curve: $\xi^{3/7}G/\eta V$ vs. Ca (T=20°C, RH=10%)

Figure 10: Capillary number at criticality versus e/R

FIGURE 1

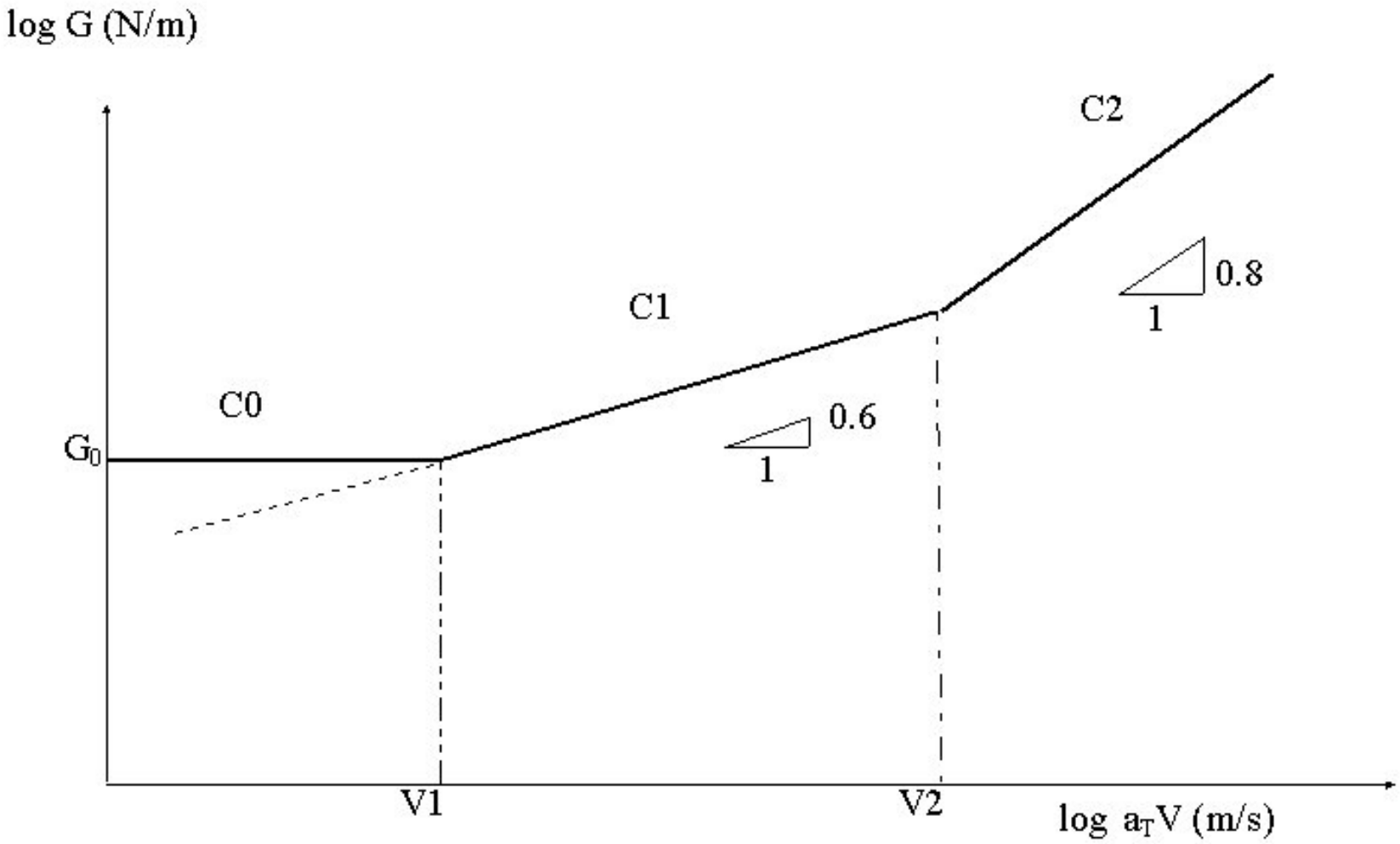

FIGURE 2

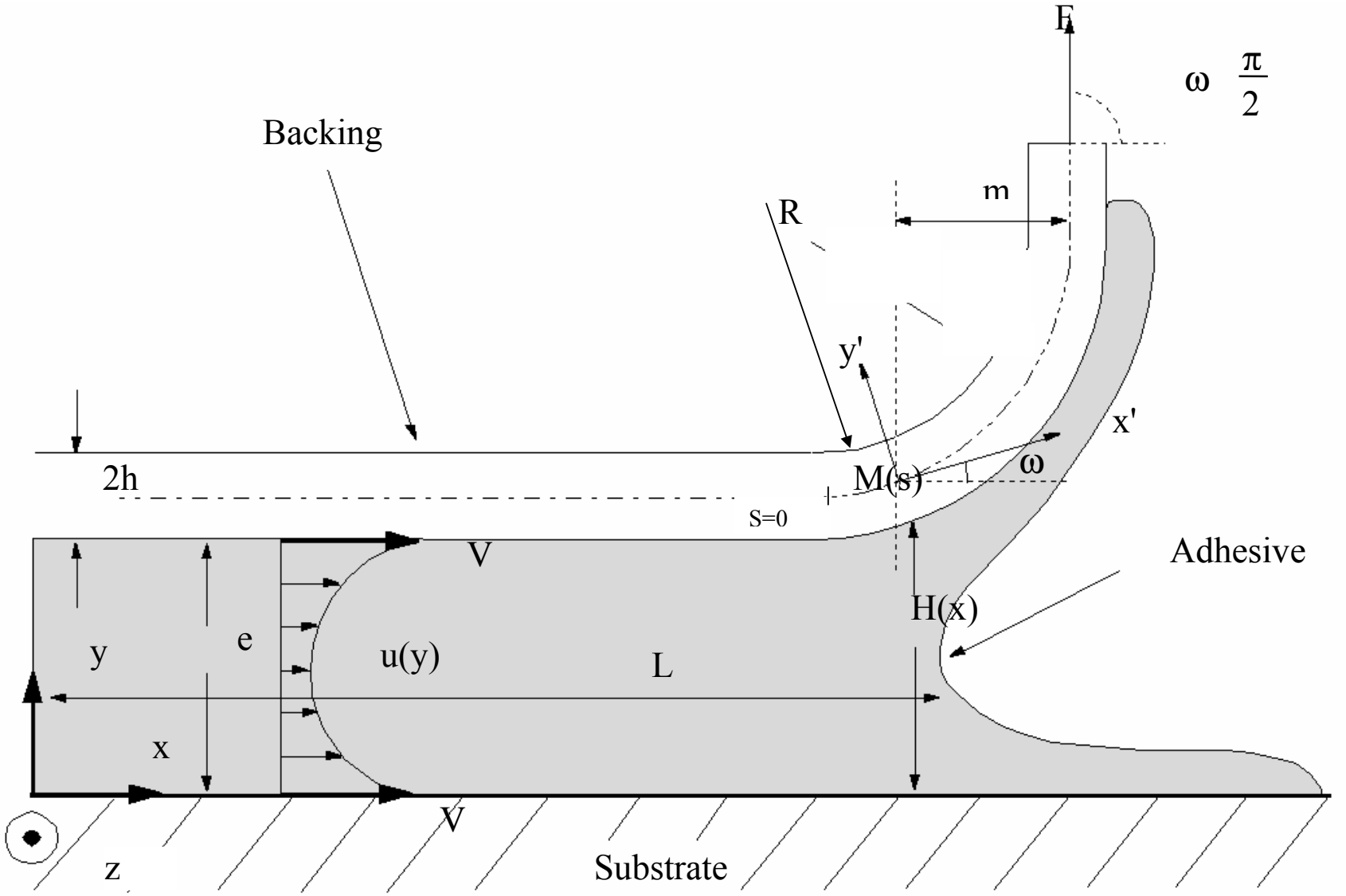
F
ω π/2
Backing
m
R
y'
x'
2h
M(s)
ω
S=0
V
Adhesive
H(x)
y
e
u(y)
L
x
V
z
Substrate

FIGURE 3

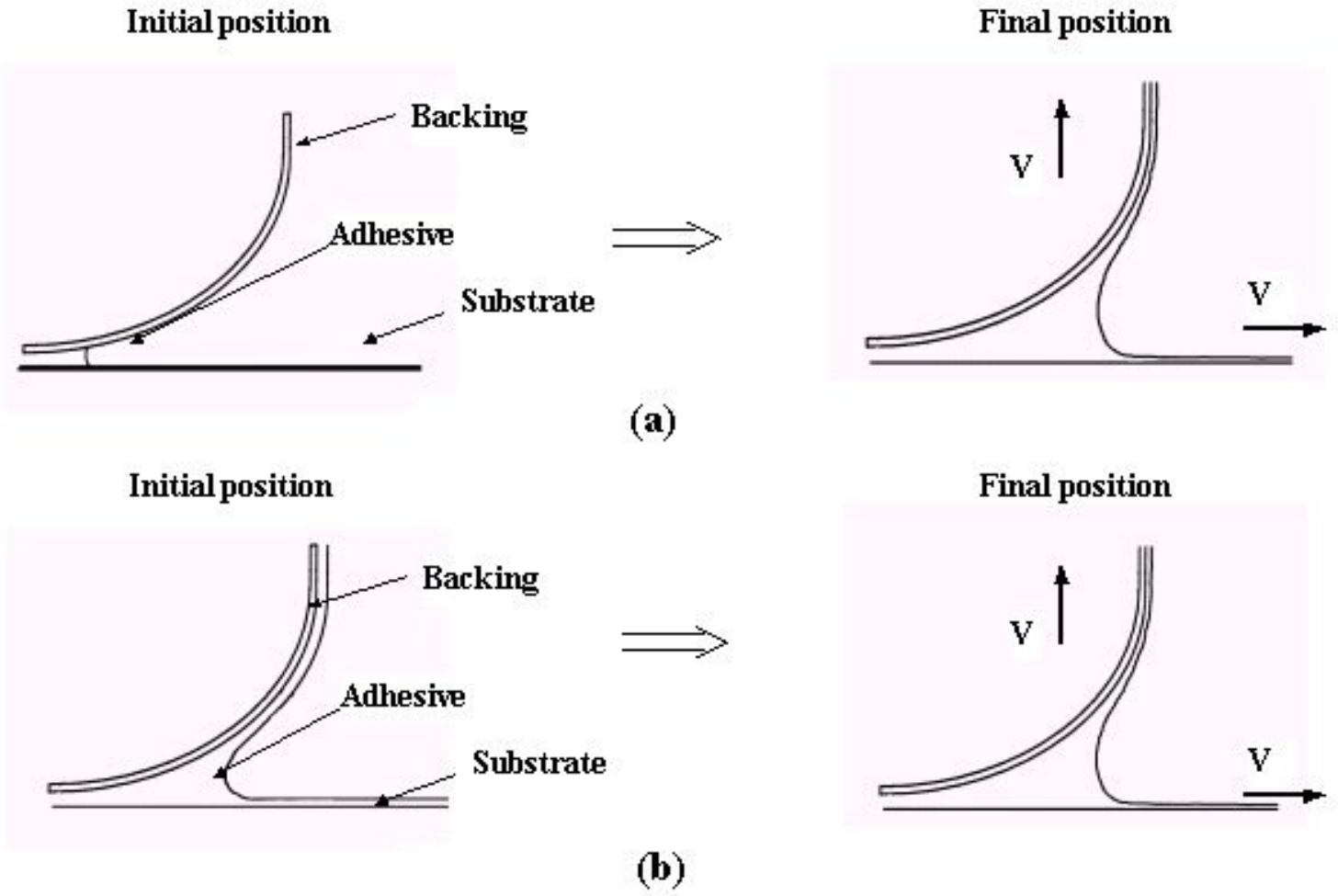
Initial position
Final position
Backing
Adhesive
Substrate
V
V
(a)
Initial position
Final position
Backing
Adhesive
Substrate
V
V
(b)

FIGURE 4

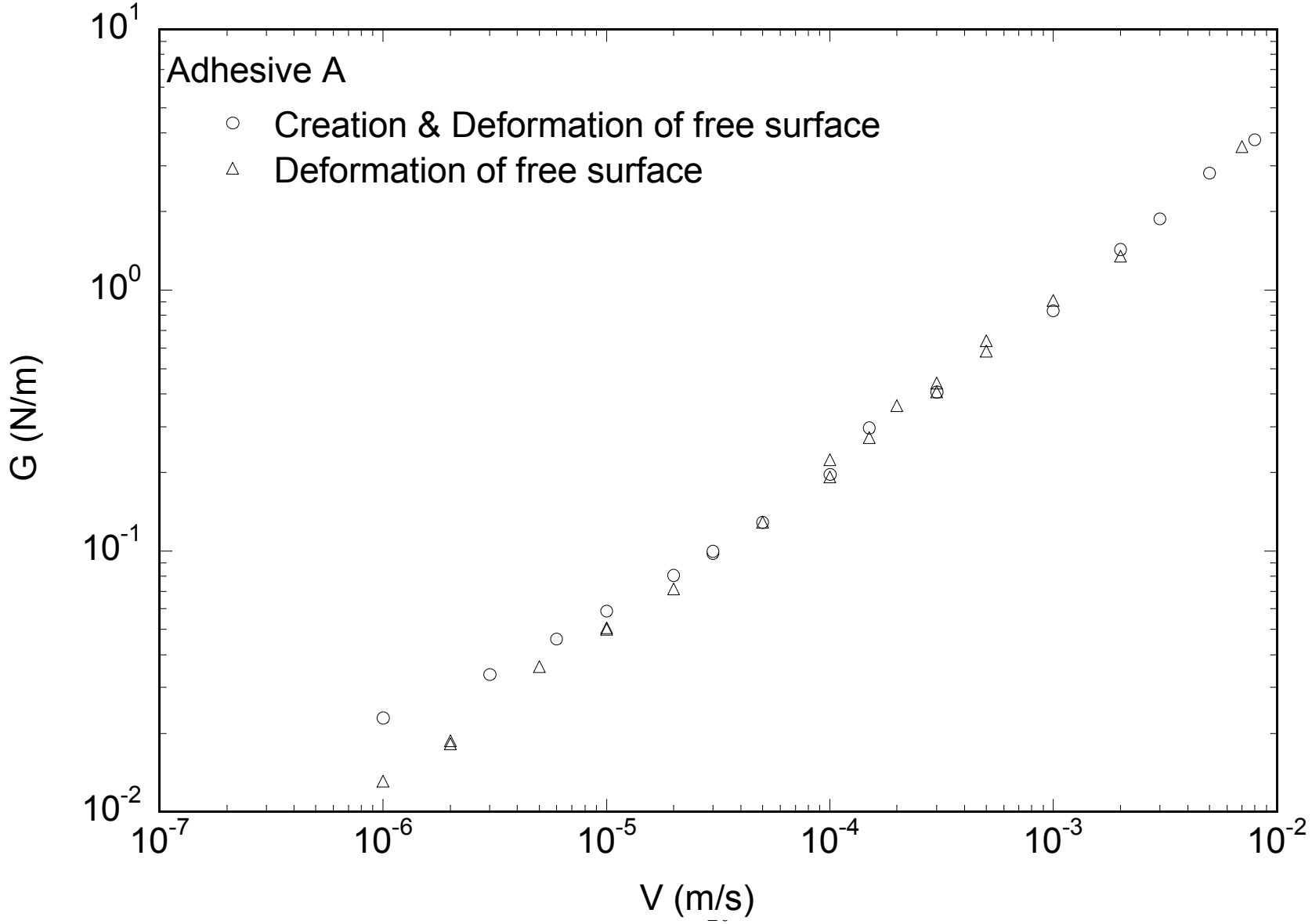
Adhesive A
Creation & Deformation of free surface
Deformation of free surface
G (N/m)
V (m/s)
10^1
10^0
10^-1
10^-2
10^-7
10^-6
10^-5
10^-4
10^-3
10^-2

FIGURE 5

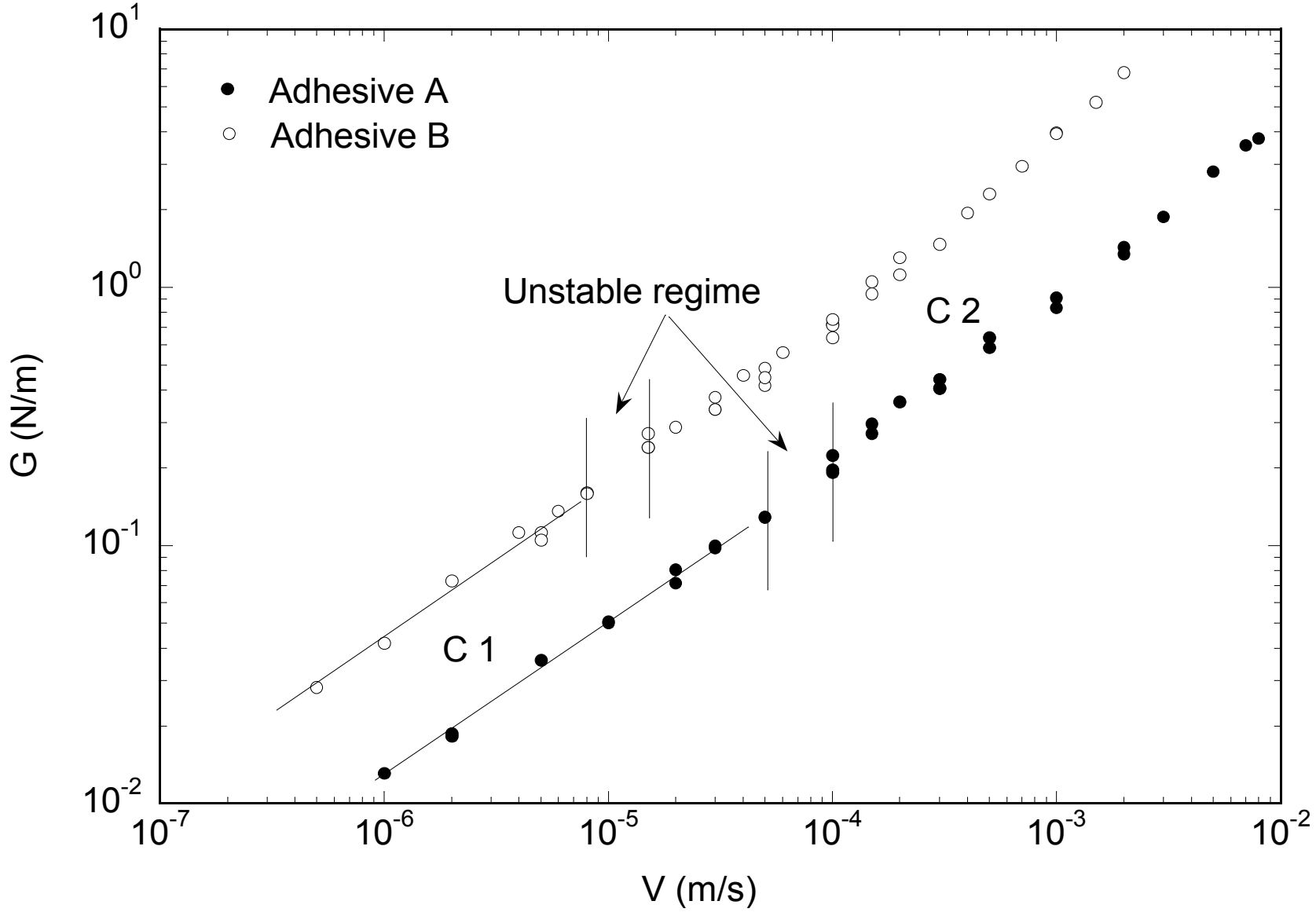
Adhesive A
Adhesive B
Unstable regime
C 1
C 2
G (N/m)
V (m/s)
10^1
10^0
10^-1
10^-2
10^-7
10^-6
10^-5
10^-4
10^-3
10^-2

FIGURE 6

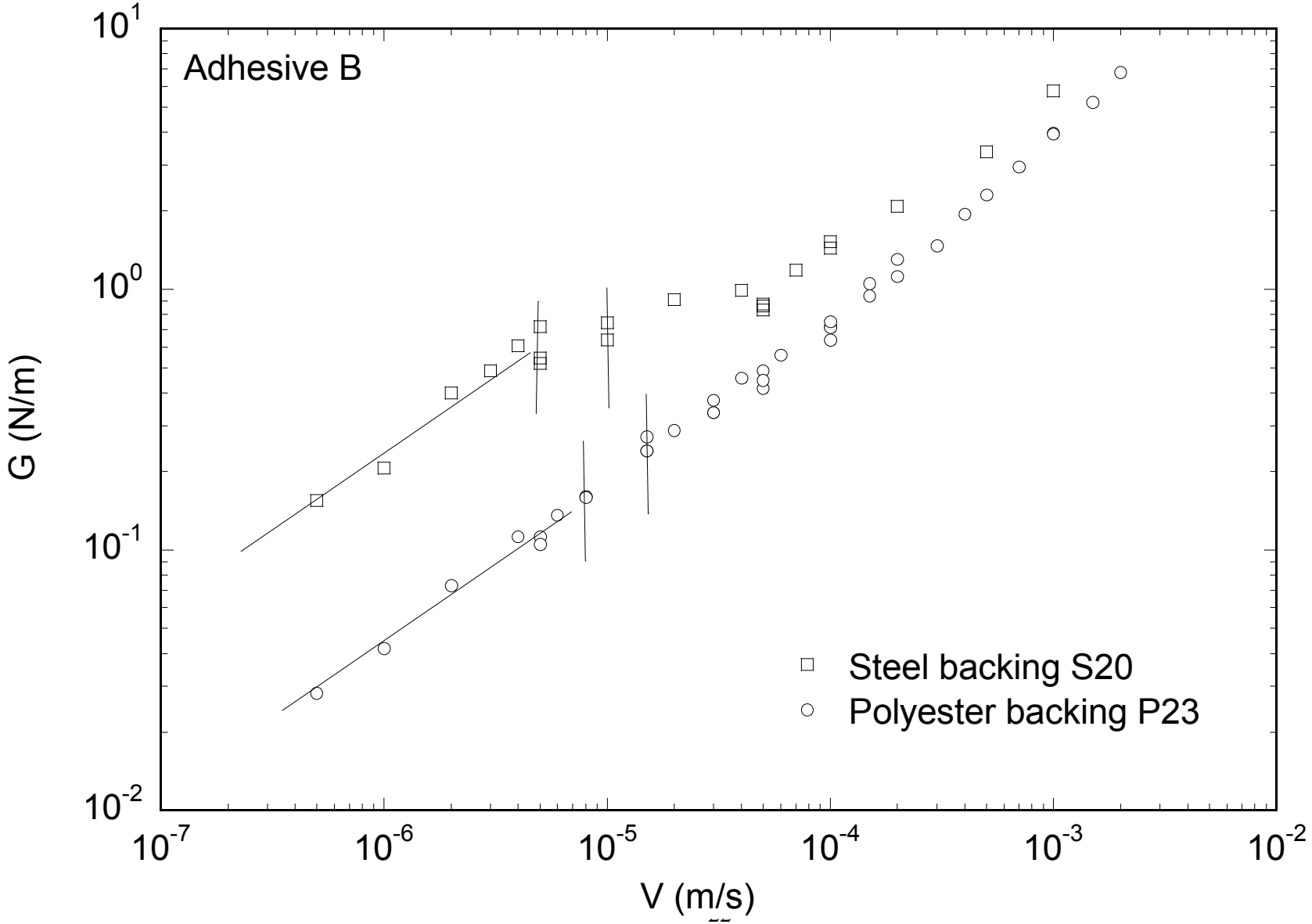
Adhesive B
G (N/m)
V (m/s)
Steel backing S20
Polyester backing P23
10^1
10^0
10^-1
10^-2
10^-7
10^-6
10^-5
10^-4
10^-3
10^-2

FIGURE 7

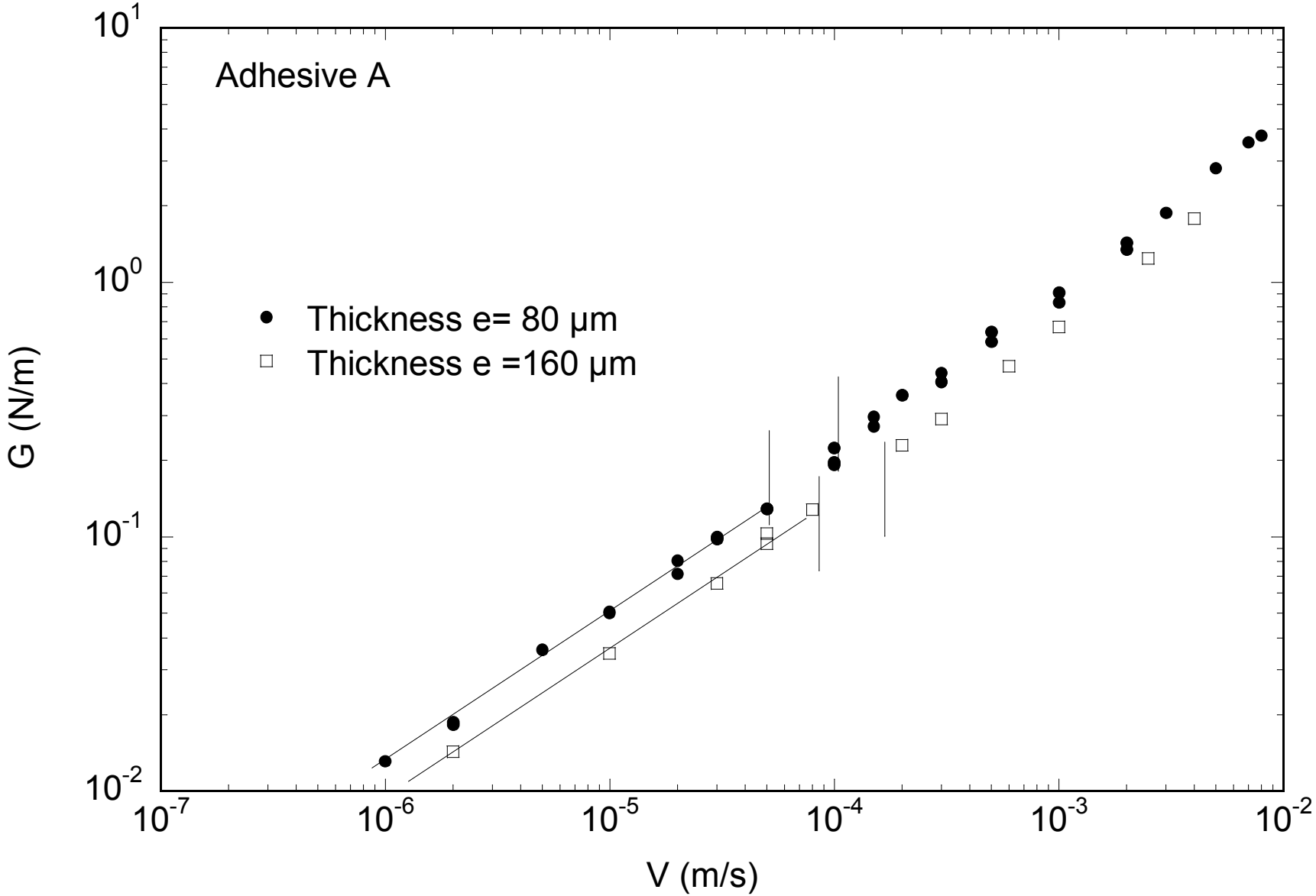
Adhesive A
Thickness e= 80 µm
Thickness e =160 µm
G (N/m)
V (m/s)
10^1
10^0
10^-1
10^-2
10^-7
10^-6
10^-5
10^-4
10^-3
10^-2

FIGURE 8

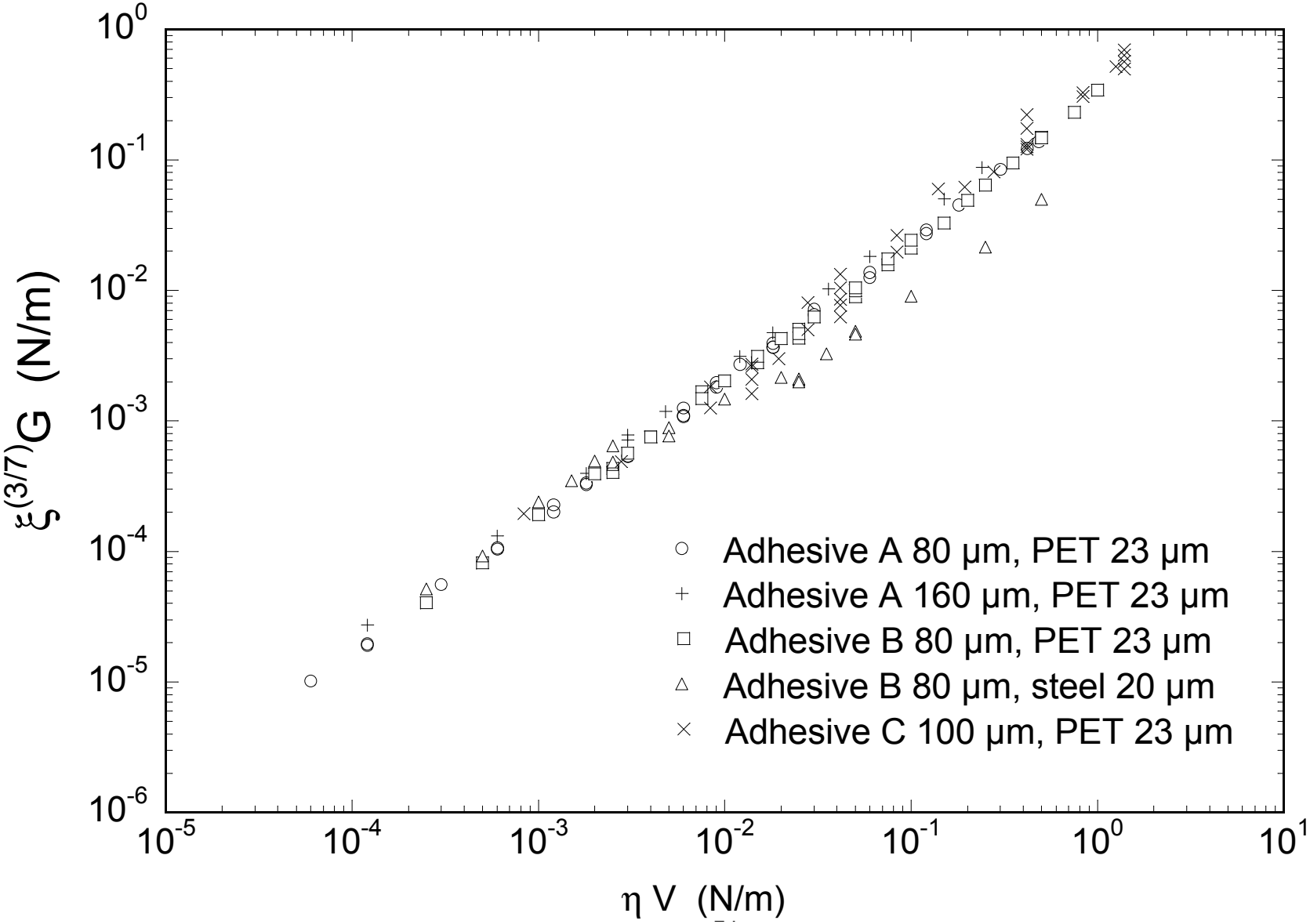
10^0
10^{-1}
10^{-2}
10^{-3}
10^{-4}
10^{-5}
10^{-6}
$\xi^{(3/7)}G$ (N/m)
10^{-5}
10^{-4}
10^{-3}
10^{-2}
10^{-1}
10^0
10^1
η V (N/m)
Adhesive A 80 µm, PET 23 µm
Adhesive A 160 µm, PET 23 µm
Adhesive B 80 µm, PET 23 µm
Adhesive B 80 µm, steel 20 µm
Adhesive C 100 µm, PET 23 µm

FIGURE 9

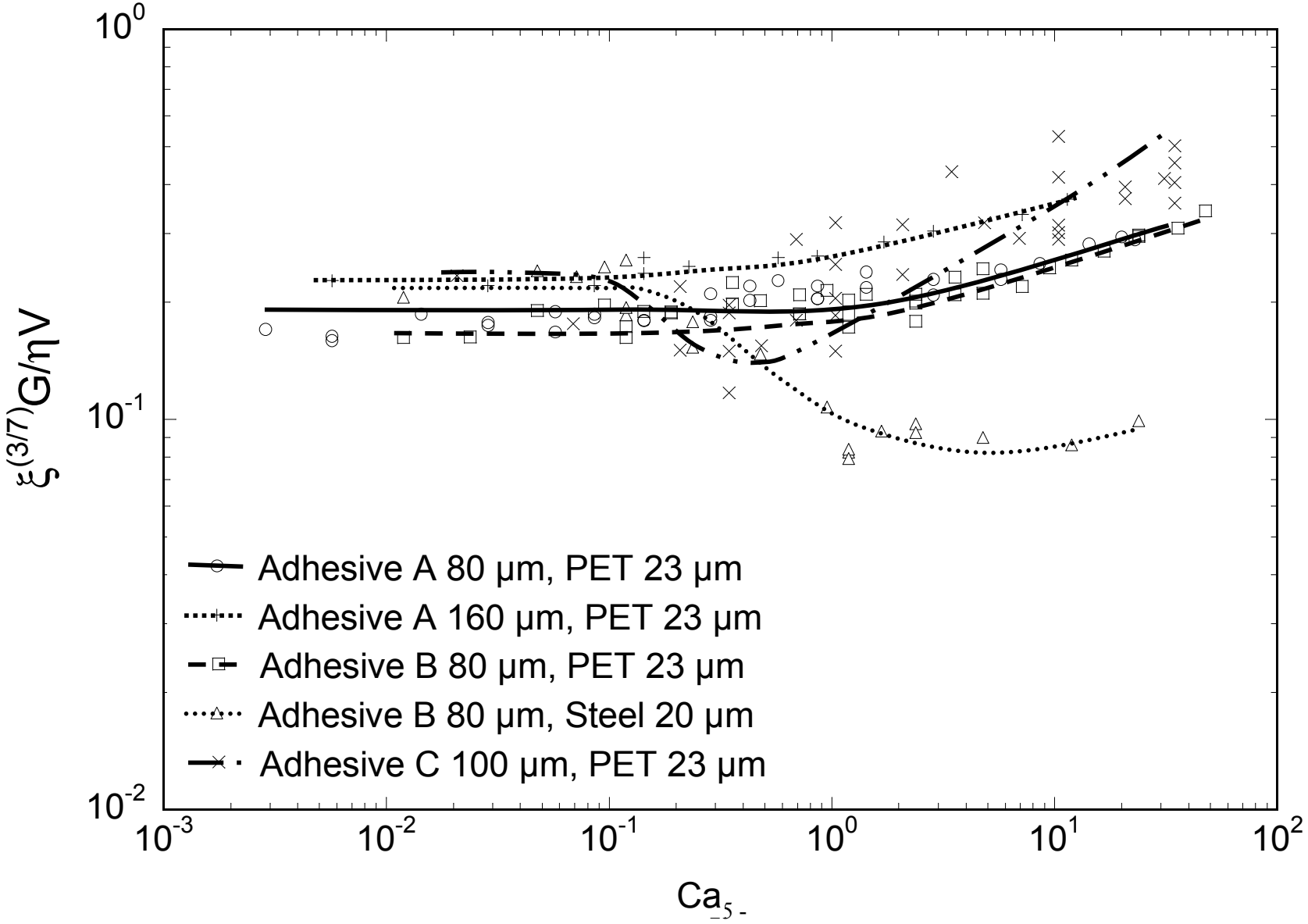
10^0
10^{-1}
10^{-2}
$\xi^{(3/7)}G/\eta V$
10^{-3}
10^{-2}
10^{-1}
10^0
10^1
10^2
Ca_{5-}
Adhesive A 80 µm, PET 23 µm
Adhesive A 160 µm, PET 23 µm
Adhesive B 80 µm, PET 23 µm
Adhesive B 80 µm, Steel 20 µm
Adhesive C 100 µm, PET 23 µm

FIGURE 10

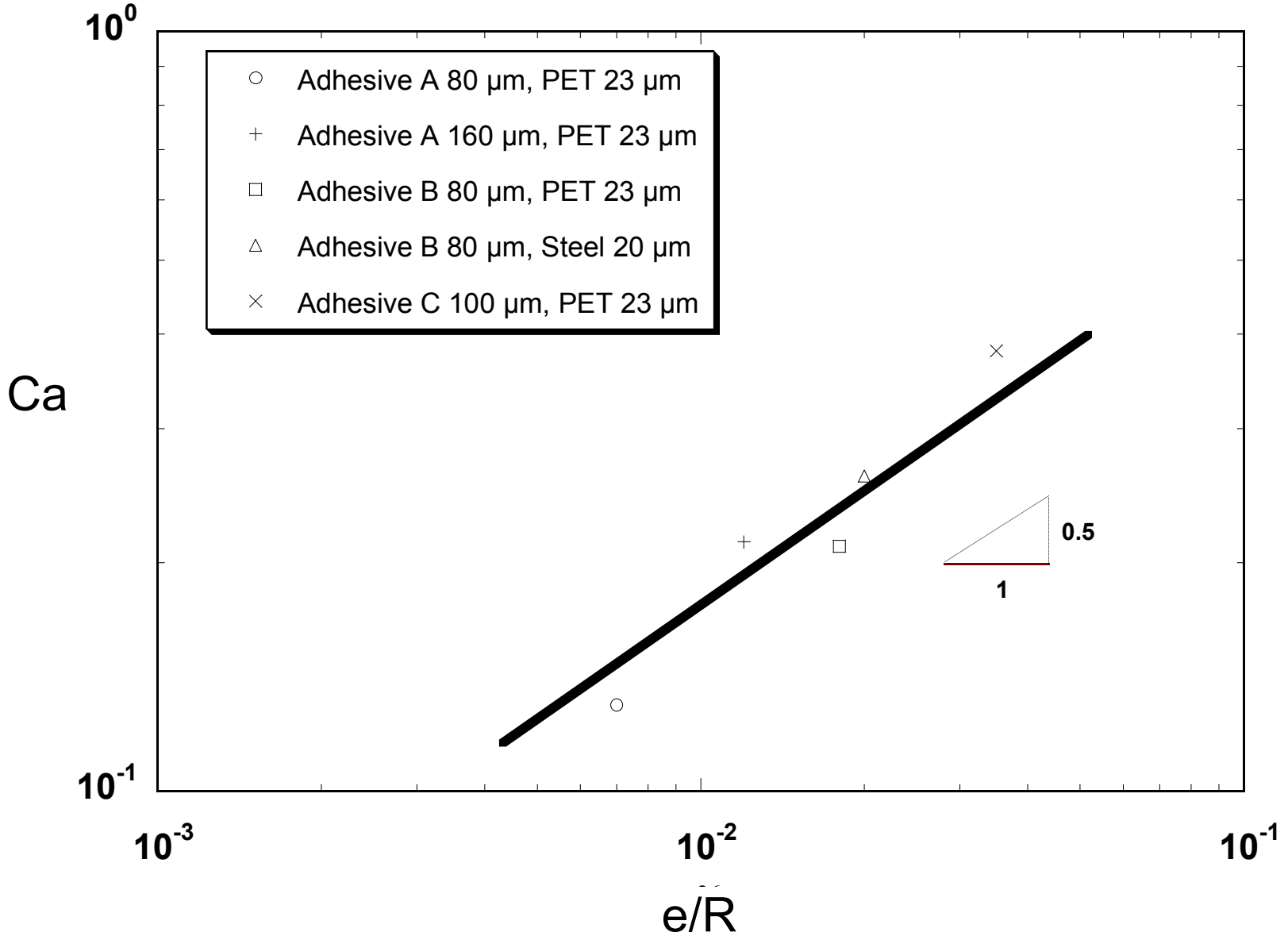
10^0
10^{-1}
10^{-3}
10^{-2}
10^{-1}
Ca
e/R
Adhesive A 80 µm, PET 23 µm
Adhesive A 160 µm, PET 23 µm
Adhesive B 80 µm, PET 23 µm
Adhesive B 80 µm, Steel 20 µm
Adhesive C 100 µm, PET 23 µm
0.5
1

TABLES

Adhesive	*A*	*B*	*C*
Origin	Fluid 47 V 60 000 Rhodia	Fluid 47 V 500 000 Rhodia	Pharmaceutical
Composition	Polydimethyl-siloxane	Polydimethyl-siloxane	20% copolymer + 40% tackifier + 40% plasticizer
Zero-shear viscosity (T=20°C)	60 Pa.s	500 Pa.s	$3.125\ 10^5$ Pa.s
Surface tension	21 mN/m	21mN/m	38.8 mN/m

Table 1: Adhesives characteristics

Backing	*P23*	*S10*	*S20*
Origin	Hoechst RN 23	Hasberg	Hasberg
Material	Polyester	Steel	Steel
Young's modulus	4.5 GPa	210 GPa	210 GPa
Thickness (2h)	23 µm	10 µm	20 µm

Table 2: Backings characteristics